ORIGINAL RESEARCH ARTICLE

Electrochemical Synthesis of Covalently Bonded Poly (3, 4-dioxyethylthiophene)–Carbon Nanotubes Composite with Enhanced Electrochromic Properties

SHANXIN XIONG [1,2,4] JIAOJIAO ZHANG,[1] XIAOQIN WANG,[1] RUNLAN ZHANG,[1] MING GONG,[1] BOHUA WU,[1] JIA CHU,[1] MENGNAN QU,[1] ZHEN LI,[1] and ZHENMING CHEN[3]

1.—College of Chemistry and Chemical Engineering, Xi'an University of Science and Technology, Xi'an 710054, People's Republic of China. 2.—Key Laboratory of Coal Resources Exploration and Comprehensive Utilization, Ministry of Natural Resources, Xi'an 710021, People's Republic of China. 3.—Guangxi Key Laboratory of Calcium Carbonate Resources Comprehensive Utilization, Hezhou University, Hezhou 542899, People's Republic of China. 4.—e-mail: xiongsx@xust.edu.cn

A Poly (3, 4-dioxyethylthiophene)–Carbon Nanotubes (PEDOT–CNT) composite electrochromic material, connected by interfacial covalent bonds, was successfully synthesized by electrochemical copolymerization of 3, 4-dioxyethylthiophene with thiophene-2-methylamine functionalized CNT. The molecular and aggregate structures of PEDOT–CNT were investigated by Fourier transform infrared spectroscopy, Raman spectroscopy, scanning electron microscopy and transmission electron microscopy. The electrochemical behavior and electrochromic properties of PEDOT–CNT were measured by CV (cyclic voltammetry), UV–Vis (ultraviolet visible spectroscopy) and EIS (electrochemical impedance spectroscopy). The test results show that the electrochromic performance of PEDOT–CNT is better than that of neat PEDOT. As the percentage of carbon nanotubes increases, the contrast and response speed of the composites increase accordingly. The PEDOT film has a contrast under square-wave potential of 0.54, a coloring time of 6.42 s, and a fading time of 2.54 s. Compared with PEDOT, the contrasts of PEDOT–CNT-3%, PEDOT–CNT-5% and PEDOT–CNT-7% are increased by 31%, 33%, and 89%, respectively. The response speeds of PEDOT–CNT-5% increase to coloring time of 3.51 s and fading time of 1.37 s.

Key words: Interface covalent bonds, PEDOT, CNTs, electrochromism

INTRODUCTION

Since Heeger and Shirakawa[1,2] discovered highly conductive doped polyacetylene films, conductive polymers (CPs)[3] have rapidly developed into a class of materials with attractive application prospects which has the advantages of light weight, good flexibility, low cost, excellent electrochemical performance and high energy efficiency.[4] Currently, CPs are mainly used in solar cells,[5,6] fuel cells,[7,8] light-emitting diodes (LEDs),[9–11] chemical and biological sensor,[12,13] supercapacitors,[14–23] electromagnetic shielding,[24] electrochromism,[25–30] stealth technology and metal anti-corrosion.[31,32]

Common conductive polymers include polyacetylene (PA),[33,34] polypyrrole (PPy),[35,36] polythiophene (PTh)[37,38] and polyaniline (PANI).[39–41] Among these, poly (3, 4-ethylenedioxythiophene) (PEDOT),[42–49] one of the common derivatives of polythiophene, is not only a typical low band gap conductive polymer, but also a much-studied cathode electrochromic material.[50] In recent years, many research works have focused on PEDOT–CNT composites Carbon nanotubes have excellent

mechanical stability, electrical properties, large specific surface area and porous structure; they improve the mechanical strength and conductivity of the composite materials and facilitate the diffusion of ions to enable fast electrochemical processes.[51–53]

Er-Chieh Cho[54] prepared a flexible transparent electrode of Au-MWCNT/PEDOT/PSS by using a simple polyol process with surfactant-assisted sonication, which has a sheet resistance of 52 Ω/sq and a contrast ratio of 86.2% at 550 nm. Ranulfo Allen[51] used an in-situ polymerization to obtain PEDOT–CNT composite films with a conductivity of 3300 S/cm. Shen[55] successfully prepared a PEDOT–CNT composite electrode by electrochemical deposition, and further assembled it into an electrochromic device with high coloring efficiency. Sathish Reddy[56] prepared a PDA @ CNTs–PEDOT hybrid membrane by electrochemical deposition, which had high charge injection capability and stability and an excellent electrochemical sensor that can be used in multifunctional bioelectrodes. However, it has been found that the interfacial interaction between PEDOT and CNT and the loading amount of CNT are two key issues for affecting the properties of PEDOT–CNT composites. For example, a high CNT concentration can dramatically decrease the transmittance of the composite and decay the contrast. Moreover, the small diameter and high surface energy of CNT makes it easy to entangle and agglomerate. The surfactant used to improve the dispersibility of CNTs also impedes the formation of the PEDOT and CNT continuous pathway.[54] To overcome this problem, we have demonstrated successfully the significant enhancement function of an interfacial covalent band between the polyaniline and carbon nanostructures (fullerene, carbon nanotube and graphene) on the electrochromic properties of PANI/carbon nanostructures composites.[57,58] The electron conduct and ion transport processes of CP can be simultaneously boosted owing to direct electron conduct through covalent bonds and the loose aggregation created by incorporation of carbon nanostructures.

In this paper, a PEDOT–CNT composite electrochromic material with interfacial covalent bonds was successfully prepared by electrochemical copolymerization of thiophene with thiophene-2-methylanine functionalized CNT. In this work, we describe in detail the preparation, structure, and properties of PEDOT–CNT composite electrochromic materials. In addition, the effects of the introduction of carbon materials on the electrochemical and electrochromic properties of PEDOT are discussed. It is proved that the special structure of nano-carbon materials has great potential for improving the electrochromic performance of conductive polymers.

EXPERIMENTAL

Synthesis of Functionalized Carbon Nanotubes (F-CNT)

Chemicals were not purified prior to use unless otherwise stated. We used multi-walled carbon nanotubes (MWCNT) with outer diameter (OD) 20-40 μm, length 10-30 μm and purity > 90 wt.%. The functionalization process of CNT was carried out in two steps. First, the MWCNTs were purified by thermal treatment. The MWCNTs were calcined in a muffle furnace at 500°C for 2 h to remove the amorphous carbon. Then, 300 mg of the calcined CNT was acidified by 75 mL of mixed acid solution (concentrated sulfuric acid: concentrated nitric acid = 3:1 (v:v)) with assistance of ultrasonication for 5 h. The acidified CNTs were washed with deionized water to pH ≈ 7. Finally, the filtrate cake was dried in a freeze-drying oven for 24 h to obtain acidified carbon nanotubes (A-CNT). The second step was the functionalization process. First, 30 mg of thiophene-2-methylamine was added to 10 mL of N,N-dimethylformamide (DMF) with assistance of sonication and designated as A. 5 mg of A-CNT was added to 50 mL of DMF with ultrasonicated dispersion for 25 min and designated as B. Then, 100 mg of N–N dicyclohexylcarbodiimide (DCC) was added to B, and subjected to 10 min ultrasonic treatment, followed by 20 min heating in an oil bath at 50°C. Finally, solution A was added to solution B. The functionalization process lasted for 24 h in oil bath at 50°C. The general functionalization process is shown in Fig. 1. The strong dehydration capacity of DCC is the key for functionalization, as shown in our previous work.[57]

Preparation of PEDOT–CNT

The electrochemical synthesis of PEDOT was attempted using different electrolyte systems, different polymerization voltages and polymerization times. With optimized synthesis condition, deposition voltage of 1.3 V, polymerization time of 30 s in 1 M LiClO$_4$/PC electrolyte, the obtained PEDOT film had uniform thickness, good stability and gloss. Therefore, under the same conditions, different mass percentages of F-CNT (with respect to the EDOT monomer) were dispersed into electrolyte, and the obtained of PEDOT–CNT films were named as PEDOT–CNT-3%, PEDOT–CNT-5% and PEDOT–CNT-7%.

Characterization

FTIR (Fourier Transform Infrared) spectra of samples were obtained on a PerkinElmer GX spectrometer using the KBr pellet method. The samples were scraped from the ITO conductive glass before the test. An InVia Reflex laser microscopic confocal Raman spectrometer was used for the Raman test.

Electrochemical Synthesis of Covalently Bonded Poly (3, 4-dioxyethylthiophene)–Carbon
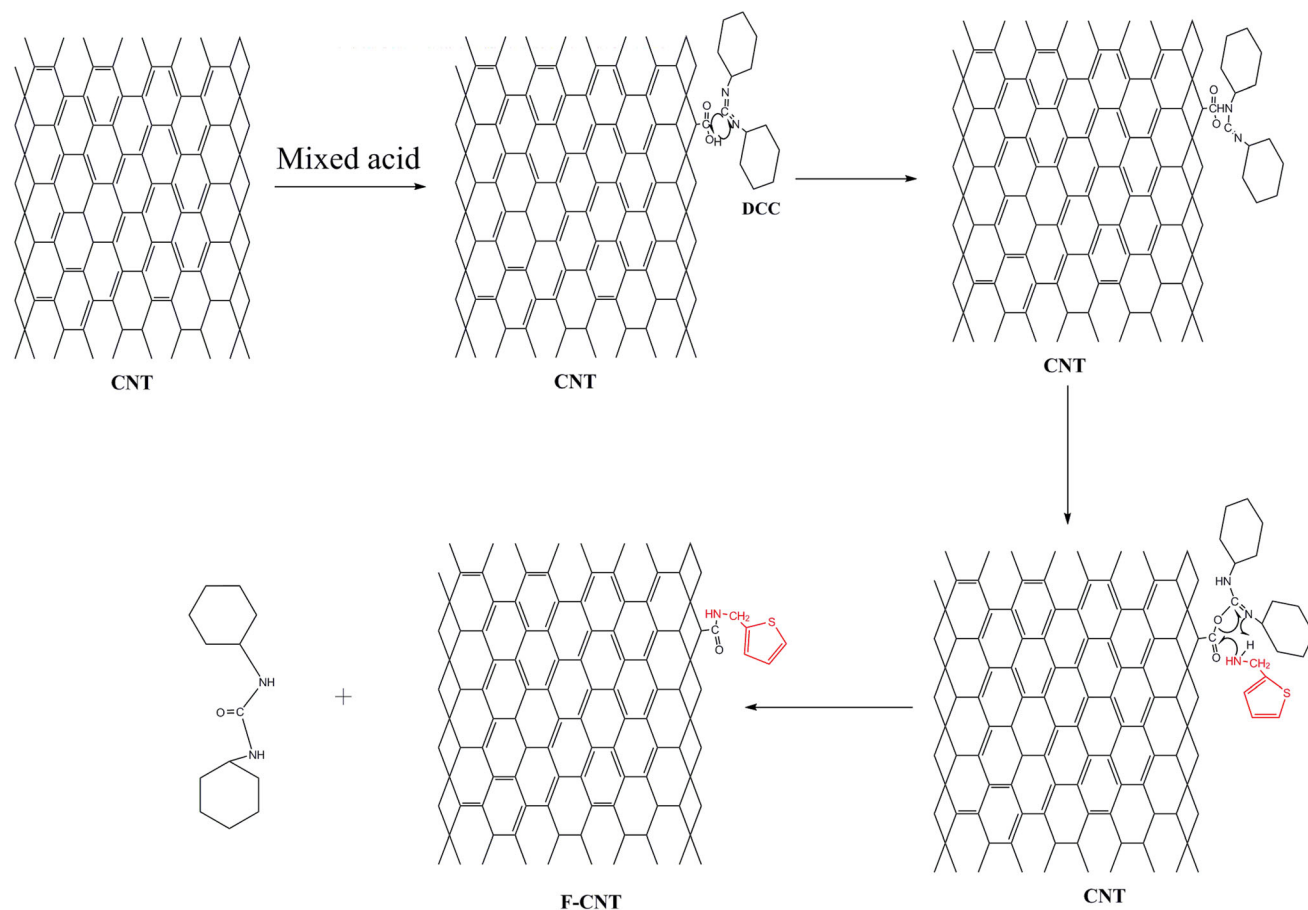Nanotubes Composite with Enhanced Electrochromic Properties

2391

Fig. 1. The reaction process of functionalized CNT (F-CNT).

The excitation light was He–Ne laser with an excitation wavelength of 532 nm, an excitation intensity of 1% and laser power of 50 mW. The morphologies of the samples were observed by scanning electron microscopy (SEM) (Phenom/Pro) and transmission electron microscopy (TEM) (JEM-2100). In-situ spectroelectrochemical properties and switching speeds of materials and devices were measured using an Autolab PGSTAT101 potentiostat in association with an UV-vis spectrometer (SHIMADZU 2550). The CV (cyclic voltammetry) and EIS tests were carried out with a three-electrode system. The working electrode was an ITO/glass electrode (17-22 Ω) coated with an electrochromic layer; the thickness of the electrochromic films was about 400-450 nm. The counter and reference electrodes were Pt plate (99.99%) and Ag/AgCl (3 M KCl), respectively, and its electrolyte was 1 M LiClO$_4$/PC (Propylene carbonate).

RESULTS AND DISCUSSION

Synthesis and Characterization of PEDOT–CNT

FTIR was used to investigate the functional groups changes of material during the functionalization process of CNTs. As shown in Fig. 2a, the CNT exhibits some absorption peaks at 2922 cm^{-1} and 2851 cm^{-1} correlating with the symmetrical stretching vibration of surface methyl group (-CH$_3$), methylene (-CH$_2$), while the vibrational peaks at 1633 cm^{-1}, 1582 cm^{-1} and 1087 cm^{-1} can be attributed to the stretching vibrations of C=O, C=C and C-C groups, respectively. On the infrared curve of A-CNT, the absorption peaks at 1733 cm^{-1}, 1621 cm^{-1} and 1417 cm^{-1} can be attributed to the stretching vibrations of C=O and O-H in the functional groups (such as carboxyl groups, lactone carboxyl groups and carboxylic anhydrides). As compared with CNT, the peak intensity of C=O is significantly enhanced, which also confirmed the successful preparation of A-CNT. When functionalized by thiophene-2-methylanine, the vibration peaks of F-CNT at 865 cm^{-1} can be attributed to the stretching vibration of the C-S bond of thiophene ring. This confirms that the thiophene group was successfully connected to the carbon nanotubes. The F-CNT exhibits some vibrational peaks at 1723 cm^{-1} and 1670 cm^{-1} correlating with appearance of C=O. The vibration peak at 1500 cm^{-1} can be attributed to the stretching vibration of N-H of amide.

In Fig. 2b, we show the infrared spectra of PEDOT combined with different mass ratios of CNTs. Taking PEDOT–CNT-7% as an example,
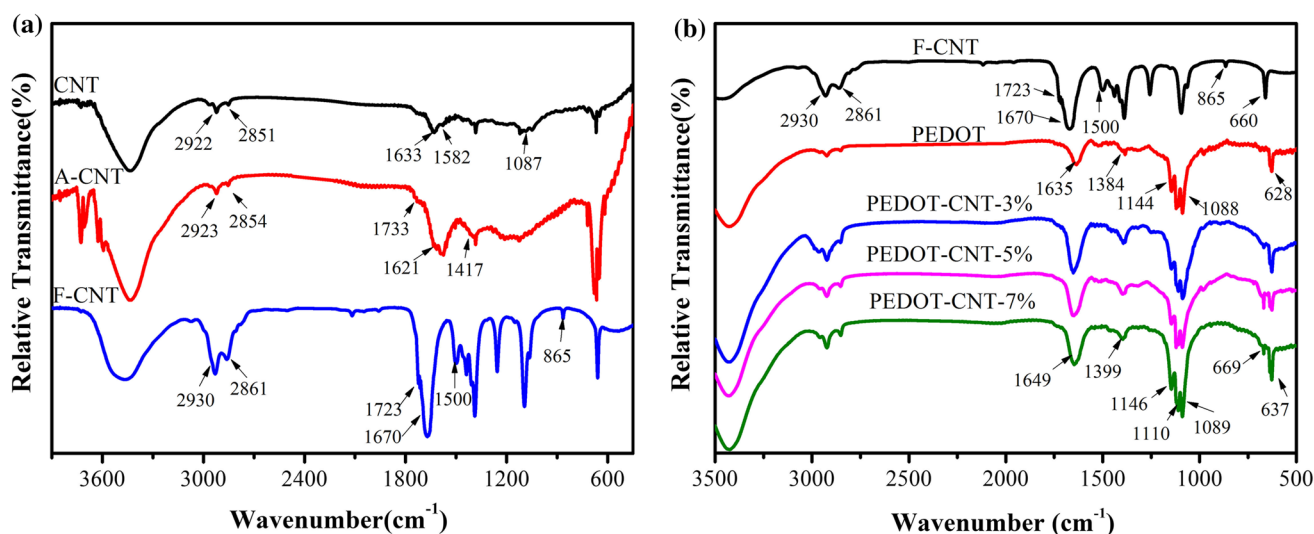
Fig. 2. FTIR spectra of CNT, A-CNT and F-CNT (a), and F-CNT, PEDOT and PEDOT–CNT (b).
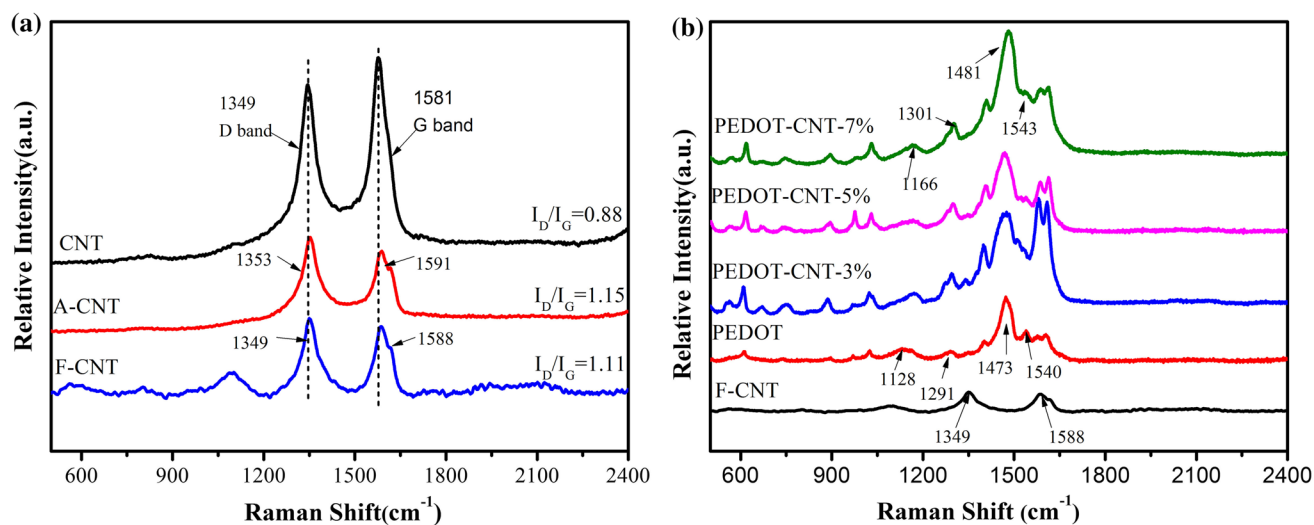

Fig. 3. Raman patterns of CNT, A-CNT, and F-CNT (a), and F-CNT, PEDOT and PEDOT–CNTs (b).

the absorption peaks at 1399 cm^{-1} and 1649 cm^{-1} are caused by the stretching vibrations of C-C and C=C on the thiophene ring. The absorption vibration peaks at 1146 cm^{-1}, 1110 cm^{-1} and 1089 cm^{-1} are attributed to the bending vibration of C-O-C in the ethylene dioxy group, and the vibration peaks at 669 cm^{-1} and 637 cm^{-1} are derived from the stretching vibration with the C-S-C. Owing to the small loading amount of F-CNTs and similar molecular structure of PEDOT and functional group of F-CNTs, the FTIR spectra of PEDOT and PEDOT–CNTs are similar. To further investigate the molecular structure of PEDOT–CNTs, Raman spectra were applied.

The chemical structures of CNTs and PEDOT–CNTs composites were analyzed using Raman analysis. For CNTs, the D peak and the G peak are very

obvious. The large I_D/I_G value indicates rich surface defects. As can be seen from Fig. 3a, the I_D/I_G value of CNTs is 0.88; after acidification treatment and functionalization process, the I_D/I_G value is increased to 1.15 for A-CNT and 1.11 for F-CNT. The strong oxidation capacity of mixed acid can destroy the ordered sp^2 hybrid structure of CNTs and introduce oxygen-containing groups into CNTs, resulting in a higher I_D/I_G ratio.[59] In the followed functionalization process, the carboxyl group on the surface of A-CNT was reacted with thiophene-2-methylamine to form an amide bond. Though the carboxyl group is converted to amide bond, the sp^2 hybrid structure is not restored. So the change of I_D/I_G value of F-CNT is not obvious.

Figure 3b shows the Raman spectra of PEDOT–CNT with different CNT contents. On the Raman

Electrochemical Synthesis of Covalently Bonded Poly (3, 4-dioxyethylthiophene)–Carbon Nanotubes Composite with Enhanced Electrochromic Properties

2393

curve of PEDOT, the C=C tensile vibration peak appears at 1540 cm^{-1} and 1473 cm^{-1}. The vibration peaks at 1291 cm^{-1} and 1128 cm^{-1} are attributed to the telescopic vibrations of the C-C inner ring and C-O in PEDOT, respectively. Compared with PEDOT, the peak positions of PEDOT–CNTs composites shifted in the large wavenumber direction. Taking PEDOT–CNT-7% as an example, the peak of the C=C symmetric stretching vibration shifts to 1543 cm^{-1} and 1481 cm^{-1}, the peak of the inner ring of C-C shifts to 1301 cm^{-1}, and the vibration peak of C-O shifts to 1166 cm^{-1} with the increase of CNTs loading amounts. These results demonstrate the influence of strong interfacial interactions, including covalent bond, π–π conjugated interactions and van der Waals forces.[60]

Figure 4 shows morphologies of F-CNT (a), PEDOT (b) and PEDOT–CNT (c, d). It can be seen from Fig. 4a, that the functionalized CNT possesses uniform structure with curly shape. The electrochemically polymerized PEDOT shows porous structure composed of nanoparticles (Fig. 4b). The PEDOT–CNT film has a porous structure similar to PEDOT, while the PEDOT nanoparticle is attached on the surface of CNTs with smaller particle size. The curly CNT with uniform dispersion in the PEDOT matrix can be verified by the TEM image (Fig. 4d). In the typical structure, the PEDOT nanoparticle is connected with CNTs through interfacial covalent bond, and the CNTs are dispersed uniformly in the matrix of PEDOT owing to its relative lower content. Thus, the interfacial electron conduct between PEDOT and CNTs benefits from its strong interfacial interaction and uniform dispersion. Also, the high ion mobility can be rendered by its porous structure. As the result, the electrochemical and electrochromic

properties can be improved by its good conduction and high mass transfer.

Electrochemical and Electrochromic Properties of PEDOT–CNT

In order to optimize the synthesis conditions of PEDOT–CNT, the effect of polymerization times on the electrochromic properties of samples with different CNT loading amounts were studied. With different synthesis times, the thickness and surface appearance of the films varied. The thickness of the film is increased with the increase of electrochemical deposition time, while the surface appearance of the film becomes uneven and rough with long deposition time (40 s). The optical contrast of electrochromic films under potentials from − 3.0 V to 2 V are listed in Table I.

During the constant voltage polymerization, with the polymerization time increased, the thickness of the film is gradually increased, and the contrast is also increased owing to increased active material. Though this increased trend of contrast is still maintained with polymerization time of 40 s, the film cannot be kept uniform owing to fragility of thick film. Considering the good uniformity and excellent stability of film obtained with 30 s polymerization time, the electrochemical and electrochromic properties of devices were tested based on this synthesis condition. The enhanced electrochromic properties of PEDOT–CNTs can be preliminarily affirmed by comparison of the optical contrast of films with different CNT amounts.

The CV tests of PEDOT and PEDOT–CNT films obtained with 30 s polymerization time were performed at different scan rates. With the increase of scan rate, the peak current densities were also increased, indicating an increased extent of redox reaction. Using PEDOT as an example, when the scan rate was increased from 10 mV s^{-1} to 20 mV s^{-1}, 50 mV s^{-1} and 100 mV s^{-1}, the CV peak current densities of the oxidation peak and the reduction peak were 3.7303×10^{-4} A cm^{-2} and − 7.6966×10^{-4} A cm^{-2}, 7.6741×10^{-4} A cm^{-2} and − 1.1691×10^{-4} A cm^{-2}, 2.2640×10^{-3} A cm^{-2} and − 1.8719×10^{-3} A cm^{-2}, 4.5544×10^{-3} A cm^{-2} and − 3.2775×10^{-3} A cm^{-2}, respectively. The PEDOT–CNT samples with different contents of CNTs also show the same trend. Besides the current densities,
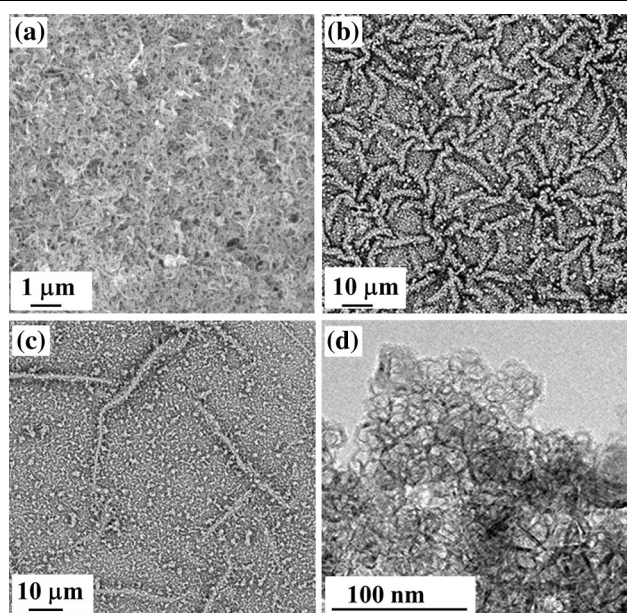

Fig. 4. SEM images of F-CNT (a), PEDOT (b), PEDOT–CNT (c), and TEM image of PEDOT–CNT (d).

Table I. The contrast of PEDOT, PEDOT–CNT-3%, PEDOT–CNT-5% and PEDOT–CNT-7% synthesized with different polymerization times

	10 s	20 s	30 s	40 s
PEDOT	0.12	0.38	0.48	0.57
PEDOT–CNT-3%	0.24	0.40	0.50	0.67
PEDOT–CNT-5%	0.29	0.40	0.54	0.67
PEDOT–CNT-7%	0.32	0.50	0.57	0.72

the redox peak locations were also shifted regularly. The oxidation peaks moved in the positive direction, while the reduction peaks move in the negative direction.

Figure 5e compares the CV curves of PEDOT and PEDOT–CNT films at the scan rate of 100 mV s^{-1}. With the introduction of carbon nanotubes, we found that the current density of the oxidation peak

and the current density of the reduction peak of PEDOT–CNT were higher than those of neat PEDOT, indicating their high electrochemical activities. The enhanced electrochemical features of PEDOT–CNT can be attributed to the high electron conduct and ion mobility brought by introduction of CNT with interfacial covalent bonds.[42] Among the samples, PEDOT–CNT-5% had the best
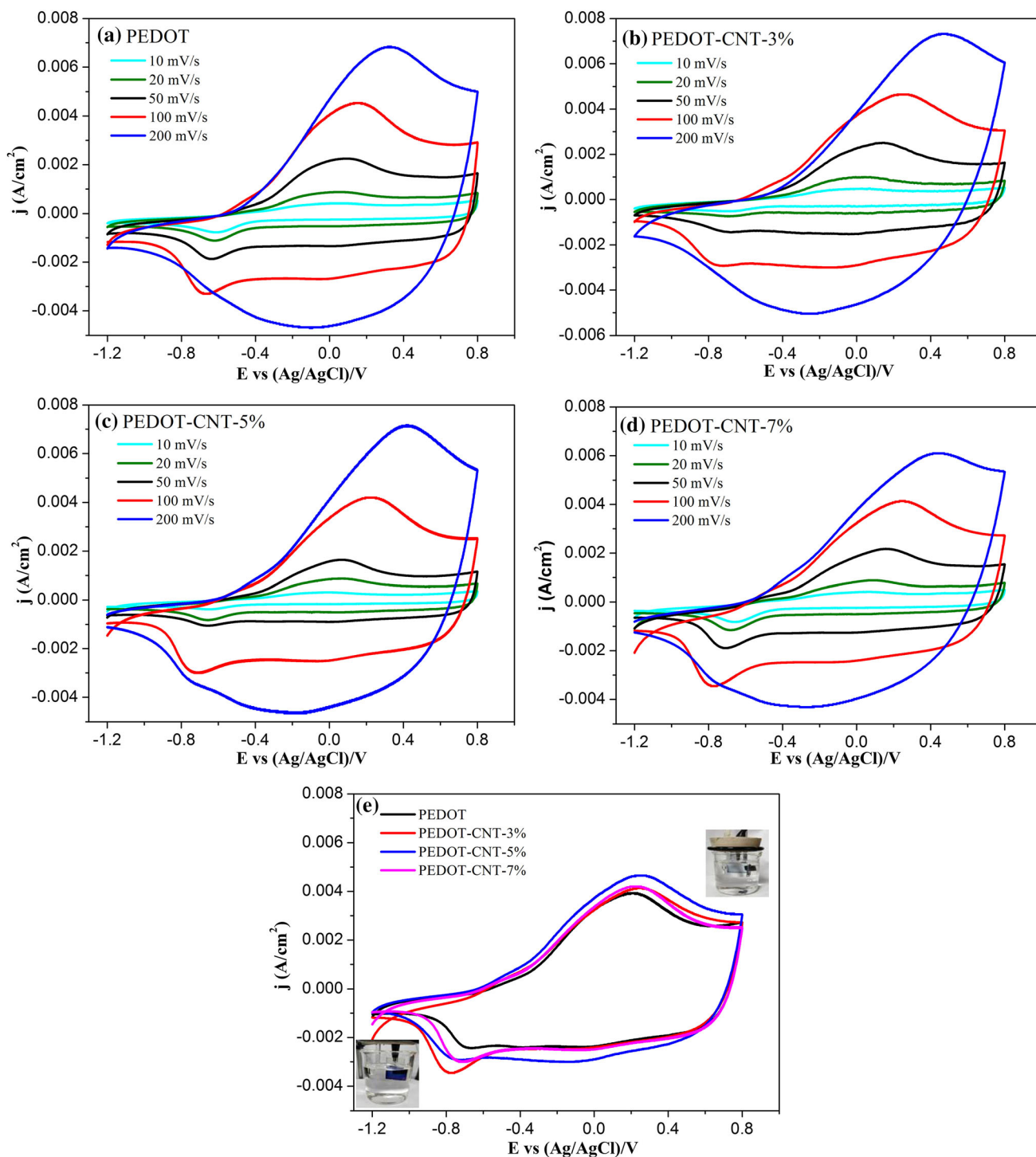

Fig. 5. CV curves of PEDOT (a) and PEDOT–CNT (b, c, d) at different scan rates, CV curves comparison at the scan rate of 100 mV s^{-1} (e) and discolored photos (The left side is the colored state under negative voltage, and the right side is the faded state under positive voltage).

Electrochemical Synthesis of Covalently Bonded Poly (3, 4-dioxyethylthiophene)–Carbon Nanotubes Composite with Enhanced Electrochromic Properties

2395

electrochemical performance, which is also consistent with the electrochromic test results. During the CV test, with the cycling change of potentials, the color of film also changed. As shown in the inset of Fig. 5e, the PEDOT film exhibited light blue under positive voltage and dark blue under negative voltage.

The electrochromic properties of PEDOT and PEDOT–CNT were tested based on a sandwich device using PEDOT and PEDOT–CNT as active layers, gel electrolyte as ion transport layer and ITO glass as electrode. Owing to the cathodic coloration feature of PEDOT, all devices showed low absorbance in the whole visible range under positive potential. While under negative potential, there was a strong absorbance peak appearing at 630 nm and the device gave a dark blue color as shown in the inset of Fig. 6c. As labeled in Fig. 6, the contrasts of the PEDOT–CNTs are higher than that of the neat PEDOT. When the voltage varied between – 3 V and 2 V, the contrast of PEDOT at the reference wavelength of 624 nm was 0.48. With the increase of CNTs amounts, the contrasts under constant voltage of PEDOT–CNTs increased by 4.2%, 12.5% and 18.8% for PEDOT–CNT-3%, PEDOT–CNT-5% and

PEDOT–CNT-7%, respectively. The enhanced contrast can be attributed to the high electron conduction brought by the three-dimensional conducting
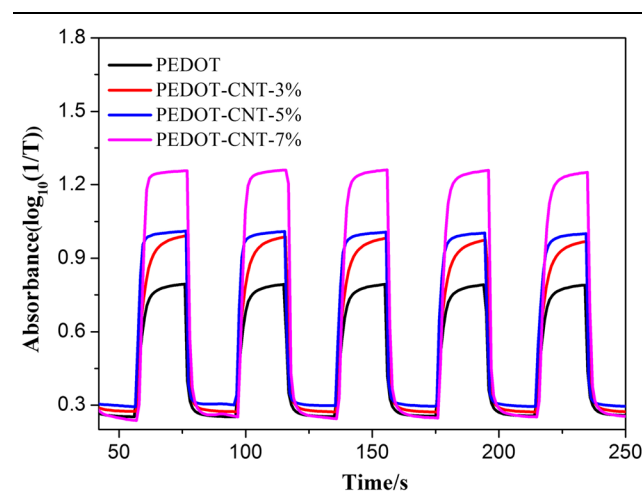

Fig. 7. Dynamic test of devices using PEDOT and PEDOT–CNT as active layers at a reference wavelength of 630 nm.
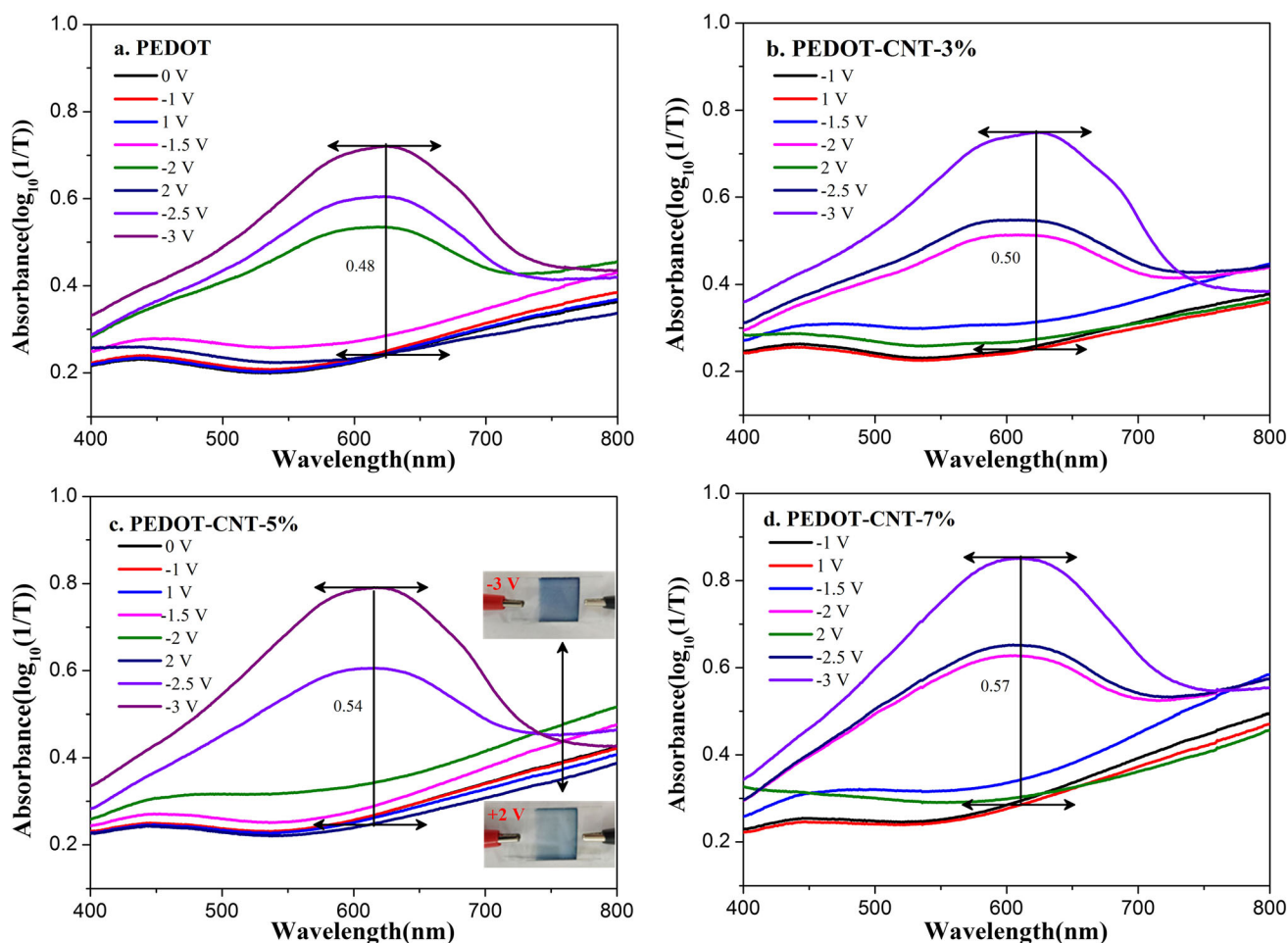

Fig. 6. Absorption spectra of devices using PEDOT (a) and PEDOT–CNT (b, c, d) as active layers with different F-CNT loading amounts.

Table II. The contrast and switching speed of PEDOT and PEDOT–CNT

	Contrast under constant voltage (ΔA)	Contrast under square-wave potential (ΔA)	Coloring time (s)	Bleaching time (s)
PEDOT	0.48	0.54	6.42	2.54
PEDOT–CNT-3%	0.50	0.71	6.21	1.93
PEDOT–CNT-5%	0.54	0.72	3.51	1.37
PEDOT–CNT-7%	0.57	1.02	4.68	2.38

Table III. The electrochromic contrast of PEDOT and its derivatives in the literature

No.	Activte material/substrate	Contrast (ΔT) (%)	Preparation methods	References
1	PEDOT–CNT/ITO-glass	40.9	Electropolymerization	[This work]
2	PEDOT-ITO/PET-80	28.8	Templated electrodeposition	42
	PEDOT/CNT-PET-86	31.3		
	PEDOT/CNT-PET-73	33.6		
	PEDOT/CNT-PET-50	35.6		
3	PEDOT/FTO-glass	35	Electrodeposition	43
	PEDOT-ZnO/FTO-glass	27		
4	PEDOT/ITO-glass	46	Electrodeposition	44
	ProDOT$_2$-EDOT$_2$/ITO-glass	75		
	ProDOT/ITO-glass	71		
5	PEDOT/ITO-glass	54	Electrodeposition	45
	PProDOT/ITO-glass	66		
	PProDOT-Me$_2$/ITO-glass	76		
6	PEDOT/ITO-glass	44	Electropolymerization	46
	PBEBT/ITO-glass	53		
7	PEDOT-HPC/ITO-glass	22	Electrodeposition	47
8	PProDOS/ITO-glass	51	Electrodeposition	48
	PProDOT/ITO-glass	54		
	PEDOS/ITO-glass	55		
	PEDOT/ITO-glass	54		
9	Star poly(3,4-ethylenedioxythiophene)-2, 5-didodecy-loxybenzene) (SPEB)/ITO-glass	43	Reflux reaction	49

network of CNTs, and directly connected covalent bonds between CNTs and PEDOT. In the electro-chemical polymerization, the F-CNTs dispersed in the electrolyte cannot react with monomer and deposit on the ITO glass electrode. So the actual content of CNTs in the PEDOT–CNT film is not equal to the loading amount. With 7% CNT loading, the bleaching curve under positive potential is slightly higher than that of other samples. This was caused by the dark color of CNTs. So the loading amount of CNTs was not increased further. Also, it can be noticed that the enhanced degree of contrast is not medium, as we applied a relative lower negative potential in constant voltage test.

When a higher potential was applied, all samples showed a much higher absorbance.

Figure 7 shows the optical response curves of devices under the step potentials between − 3.5 V and 2 V. It can be seen that all four devices can realize reversible color change in response to changes in step potential. Compared to the constant voltage test (Fig. 6), the absorbance and contrast of the four devices increased. In keeping with the short potential application time, a higher potential (− 3.5 V) was used. Under the step potential, the PEDOT–CNT devices show improved contrast. Compared with PEDOT (0.54), the contrasts were increased to 0.71, 0.72 and 1.02 for PEDOT–CNT-

Electrochemical Synthesis of Covalently Bonded Poly (3, 4-dioxyethylthiophene)–Carbon Nanotubes Composite with Enhanced Electrochromic Properties
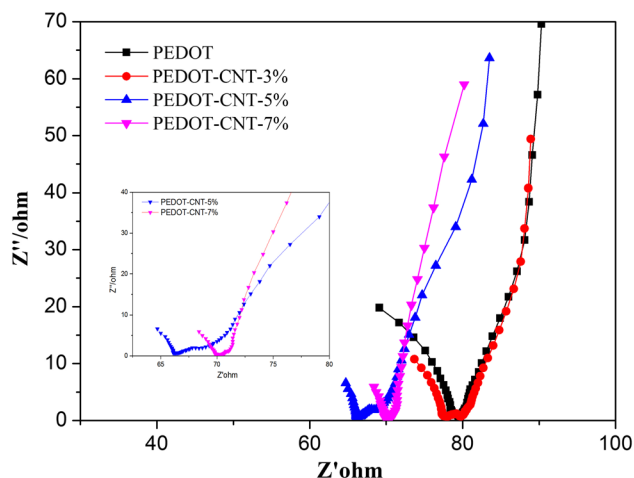
2397

Fig. 8. Nyquist plots of PEDOT and PEDOT–CNT.

3%, PEDOT–CNT-5% and PEDOT–CNT-7%, respectively. The contrasts of the materials can also be expressed in terms of transmittance ($A = \log 10 \wedge (1/T)$). Taking PEDOT–CNT-5% as an example, the contrast is 40.9% (ΔT). Table II lists the contrast of PEDOT and its derivatives in the literature. By way of comparison, we found that the electrochromic device we prepared has upper middle performance. With the increasing of CNT loading amounts, the response speed at first increases, and then decreases for PEDOT–CNT-7%. PEDOT–CNT-5% has the shortest coloring time (3.51 s) and fading time (1.37 s) among the four devices. With 7% CNT loading, the response times are increased slightly. The response time is relative to the ion transport ability of the active layer, so EIS, which can reflect the electron and ion conductivity, is used for analyzing the influence of CNTs on the mass transfer process during the operation of these electrochromic devices (Table III).

Figure 8 shows the impedance test for PEDOT and PEDOT–CNT films. The diameter of the semicircle at the left represents the charge transfer resistance of the material. As the amount of CNTs added in the PEDOT–CNT increases, the semicircle diameters decrease from 31.57 Ω (PEDOT) to 22.43 Ω (PEDOT–CNT-3%) and 20.92 Ω (PEDOT–CNT-5%), then increase slightly to 21.58 Ω (PEDOT–CNT-7%). The decrease of charge transfer resistance can be attributed to the high electrical conductivity, while, the slight increase can be attributed to the fact that overloading CNT cannot further increase the electron conduction of PEDOT–CNT, but can affect the ion transport pathway. So the integrated effect is a slight increase of charge transfer resistance, which is consistent with the CV test and response time. In short, we demonstrate an effective approach for enhancing the electrochemical and electrochromic properties of conducting

polymer using covalent bonded PEDOT–CNT synthesized by an electrochemical polymerization method, a promising strategy for synthesizing other organic-inorganic composites.

CONCLUSIONS

In summary, the PEDOT–CNT composite electrochromic material with interfacial covalent bonds was successfully prepared by electrochemical polymerization of PEDOT and functionalized carbon nanotubes. The test results show that the electrochromic performance of PEDOT–CNT is significantly better than that of neat PEDOT. As the percentage of CNTs increases, the contrast and response speed of the composites increase accordingly. The PEDOT based device has a contrast ratio of 0.54, a coloring time of 6.42 s, and a fading time of 2.54 s. Compared with PEDOT, the contrasts of PEDOT–CNT were increased by 31%, 33% and 89% for different CNT amounts. Though overloading CNTs has positive influence on the contrast, the transparency at its bleaching state and response speed were affected. We attribute these results to the dark color of CNTs and the ion hindering effect of overloading CNTs. When CNTs are added in a suitable amount, the electrochemical and electrochromic properties of PEDOT can be enhanced.

ACKNOWLEDGMENTS

CONFLICT OF INTEREST

The authors declare no conflict of interest.

REFERENCES

1. H. Shirakawa, H. Shirakawa, *Appl. Phys.*, 2001, **1**, p 281.
2. H. Shirakawa, A.G. MacDiarmid, and A.J. Heeger, H. Shirakawa, A.G. MacDiarmid, and A.J. Heeger, *J. Chem. Soc. Chem. Commun.*, 1977, **16**, p 578.
3. K. Akagi, K. Akagi, *Bull. Chem. Soc. Jpn.*, 2019, **92**, p 1509.
4. Y. Yang, W. Yuan, S. Li, X. Yang, J. Xu, and Y. Jiang, Y. Yang, W. Yuan, S. Li, X. Yang, J. Xu, and Y. Jiang, *Electrochim. Acta*, 2015, **165**, p 323.
5. T. Sakata, N. Ikeda, T. Koganezawa, D. Kajiya, and K.I. Saitow, T. Sakata, N. Ikeda, T. Koganezawa, D. Kajiya, and K.I. Saitow, *J. Phys. Chem. C*, 2019, **123**, p 20130.
6. H. Zhou, J. Cui, J. Guo, S. Tao, X. Gao, M. Liu, and M. Wang, H. Zhou, J. Cui, J. Guo, S. Tao, X. Gao, M. Liu, and M. Wang, *ACS Omega*, 2019, **4**, p 15097.
7. H. Zhang, and P.K. Shen, H. Zhang, and P.K. Shen, *Chem. Rev.*, 2012, **112**, p 2780.
8. Y.J. Wang, D.P. Wilkinson, and J. Zhang, Y.J. Wang, D.P. Wilkinson, and J. Zhang, *Chem. Rev.*, 2011, **111**, p 7625.
9. C. Song, Z. Zhong, Z. Hu, J. Wang, L. Wang, L. Ying, J. Wang, and Y. Cao, C. Song, Z. Zhong, Z. Hu, J. Wang, L. Wang, L. Ying, J. Wang, and Y. Cao, *Org. Electron.*, 2016, **28**, p 252.

10. L. Zhao, S. Wang, J. Ding, and L. Wang, L. Zhao, S. Wang, J. Ding, and L. Wang, *ACS Omega*, 2019, **4**, p 15923.

11. W.H. Kim, A.J. Mäkinen, N. Nikolov, R. Shashidhar, H. Kim, and Z.H. Kafafi, W.H. Kim, A.J. Mäkinen, N. Nikolov, R. Shashidhar, H. Kim, and Z.H. Kafafi, *Appl. Phys. Lett.*, 2002, **80**, p 3844.

12. S. Nambiar, and J.T. Yeow, S. Nambiar, and J.T. Yeow, *Biosens. Bioelectron.*, 2011, **26**, p 1825.

13. J.M. Moon, N. Thapliyal, K.K. Hussain, R.N. Goyal, and Y.B. Shim, J.M. Moon, N. Thapliyal, K.K. Hussain, R.N. Goyal, and Y.B. Shim, *Biosens. Bioelectron.*, 2018, **102**, p 540.

14. R. Yuksel, S.C. Cevher, A. Cirpan, L. Toppare, and H.E. Unalan, R. Yuksel, S.C. Cevher, A. Cirpan, L. Toppare, and H.E. Unalan, *J. Electrochem. Soc.*, 2015, **162**, p 2805.

15. R. Yuksel, A. Ekber, J. Turan, E. Alpugan, S.O. Hacioglu, L. Toppare, A. Cirpan, G. Gunbas, and H.E. Unalan, R. Yuksel, A. Ekber, J. Turan, E. Alpugan, S.O. Hacioglu, L. Toppare, A. Cirpan, G. Gunbas, and H.E. Unalan, *Electroanalysis*, 2018, **30**, p 266.

16. S. Xiong, N. Yang, X. Zhang, R. Wang, Y. Lu, H. Li, J. Liu, and S. Li, S. Xiong, N. Yang, X. Zhang, R. Wang, Y. Lu, H. Li, J. Liu, and S. Li, *J. Electron. Mater.*, 2019, **48**, p 6666.

17. S. Xiong, X. Zhang, R. Wang, Y. Lu, H. Li, J. Liu, S. Li, Z. Qiu, B. Wu, and J. Chu, S. Xiong, X. Zhang, R. Wang, Y. Lu, H. Li, J. Liu, S. Li, Z. Qiu, B. Wu, and J. Chu, *J. Polym. Res.*, 2019, **26**, p 4.

18. J. Lin, S. Yan, X. Zhang, Y. Liu, J. Lian, H. Lin, and S. Han, J. Lin, S. Yan, X. Zhang, Y. Liu, J. Lian, H. Lin, and S. Han, *Nano*, 2019, **14**, p 4.

19. J. Lin, Y. Zheng, Q. Du, M. He, and Z. Deng, J. Lin, Y. Zheng, Q. Du, M. He, and Z. Deng, *Nano*, 2013, **08**, p 1350004.

20. N. Suganya, V. Jaisankar, and E.K.T. Sivakumar, N. Suganya, V. Jaisankar, and E.K.T. Sivakumar, *Int. J. Nanosci.*, 2017, **17**, p 1760003.

21. M.V. Kiamahalleh, S.H.S. Zein, G. Najafpour, S.A. Sata, and S. Buniran, M.V. Kiamahalleh, S.H.S. Zein, G. Najafpour, S.A. Sata, and S. Buniran, *Nano*, 2012, **7**, p 1230002.

22. T. Chen, G. Wang, and Q. Ning, T. Chen, G. Wang, and Q. Ning, *Nano*, 2017, **12**, p 1750061.

23. J. Kim, J.H. Kim, and K. Ariga, J. Kim, J.H. Kim, and K. Ariga, *Joule*, 2017, **1**, p 739.

24. J. Zhou, and G. Lubineau, J. Zhou, and G. Lubineau, *ACS Appl. Mater. Interfaces*, 2013, **5**, p 6189.

25. S. Xiong, P. Jia, K.Y. Mya, J. Ma, F. Boey, and X. Lu, S. Xiong, P. Jia, K.Y. Mya, J. Ma, F. Boey, and X. Lu, *Electrochim. Acta*, 2008, **53**, p 3523.

26. S. Xiong, J. Ma, and X. Lu, S. Xiong, J. Ma, and X. Lu, *Sol. Energy Mater. Sol. Cells*, 2009, **93**, p 2113.

27. S. Xiong, Y. Wang, Y. Lu, H. Li, J. Liu, S. Li, and R. Zhang, S. Xiong, Y. Wang, Y. Lu, H. Li, J. Liu, S. Li, and R. Zhang, *Polym. Bull.*, 2017, **75**, p 3427.

28. S. Xiong, R. Wang, S. Li, B. Wu, J. Chu, and M. Gong, S. Xiong, R. Wang, S. Li, B. Wu, J. Chu, and M. Gong, *J. Electron. Mater.*, 2018, **47**, p 3974.

29. T. Hwang, H. Lee, H. Kim, G. Kim, and G. Mun, T. Hwang, H. Lee, H. Kim, G. Kim, and G. Mun, *Surf. Rev. Lett.*, 2010, **17**, p 39.

30. M. Farasat, M.M. Golzan, K. Farhadi, S.H.R. Shojaei, and S. Gheisvandi, M. Farasat, M.M. Golzan, K. Farhadi, S.H.R. Shojaei, and S. Gheisvandi, *Mod. Phys. Lett. B*, 2016, **30**, p 1650175.

31. X. Wang, J. Lu, J. Li, X. Jing, and F. Wang, X. Wang, J. Lu, J. Li, X. Jing, and F. Wang, *Electroact. Polym. Corros Control*, 2003, **843**, p 254.

32. Y. Zhao, J. Ma, K. Chen, C. Zhang, C. Yao, S. Zuo, and Y. Kong, Y. Zhao, J. Ma, K. Chen, C. Zhang, C. Yao, S. Zuo, and Y. Kong, *Nano*, 2017, **12**, p 1750056.

33. E.J. Heller, Y. Yang, and L. Kocia, E.J. Heller, Y. Yang, and L. Kocia, *ACS Cent. Sci.*, 2015, **1**, p 40.

34. E.J. Moorhead, and A.G. Wenzel, E.J. Moorhead, and A.G. Wenzel, *J. Chem. Educ.*, 2009, **86**, p 973.

35. M. Maruthapandi, A.P. Nagvenkar, I. Perelshtein, and A. Gedanken, M. Maruthapandi, A.P. Nagvenkar, I. Perelshtein, and A. Gedanken, *ACS Appl. Polym. Mater.*, 2019, **1**, p 1181.

36. T.G. Yun, B.I. Hwang, D. Kim, S. Hyun, and S.M. Han, T.G. Yun, B.I. Hwang, D. Kim, S. Hyun, and S.M. Han, *ACS Appl. Mater. Interfaces*, 2015, **7**, p 9228.

37. Y. Qian, M. Guo, C. Li, K. Bi, and Y. Chen, Y. Qian, M. Guo, C. Li, K. Bi, and Y. Chen, *ACS Appl. Mater. Interfaces*, 2019, **11**, p 30470.

38. S. Velayudham, C.H. Lee, M. Xie, D. Blair, N. Bauman, Y.K. Yap, and H. Liu, S. Velayudham, C.H. Lee, M. Xie, D. Blair, N. Bauman, Y.K. Yap, and H. Liu, *ACS Appl. Mater. Interfaces*, 2010, **2**, p 104.

39. R. Zeng, Z. Li, L. Li, Y. Li, J. Huang, Y. Xiao, and Y. Chen, R. Zeng, Z. Li, L. Li, Y. Li, J. Huang, Y. Xiao, and Y. Chen, *ACS Sustain. Chem. Eng.*, 2019, **7**, p 11540.

40. Y.F. Lin, C.H. Chen, W.J. Xie, S.H. Yang, M.T. Lin, and W.B. Jian, Y.F. Lin, C.H. Chen, W.J. Xie, S.H. Yang, M.T. Lin, and W.B. Jian, *ACS Nano*, 2011, **5**, p 1541.

41. E.N. Zare, P. Makvandi, B. Ashtari, F. Rossi, A. Motahari, and G. Perale, E.N. Zare, P. Makvandi, B. Ashtari, F. Rossi, A. Motahari, and G. Perale, *J. Med. Chem.*, 2020, **63**, p 1.

42. R. Malavé-Osuna, V. Hernández, J.T. López-Navarrete, E.I. Kauppinen, and V. Ruiz, R. Malavé-Osuna, V. Hernández, J.T. López-Navarrete, E.I. Kauppinen, and V. Ruiz, *J. Phys. Chem. Lett.*, 2010, **1**, p 1367.

43. H.W.M. Fung, S. So, K. Kartub, and R.M. Corn, H.W.M. Fung, S. So, K. Kartub, and R.M. Corn, *J. Phys. Chem. C*, 2018, **123**, p 762.

44. J.F. Ponder, A.M. Österholm, and J.R. Reynolds, J.F. Ponder, A.M. Österholm, and J.R. Reynolds, *Macromolecules*, 2016, **49**, p 2106.

45. L.G. Carleton, M.W. Dean, R.D. Rauh, and J.R. Reynolds, L.G. Carleton, M.W. Dean, R.D. Rauh, and J.R. Reynolds, *Chem. Mater.*, 2002, **14**, p 3964.

46. B. Abidin, G. Gorkem, D. Asuman, and T. Levent, B. Abidin, G. Gorkem, D. Asuman, and T. Levent, *Chem. Mater.*, 2008, **20**, p 7510.

47. N. Eguchi, and H. Goto, N. Eguchi, and H. Goto, *ACS Appl. Mater. Interfaces*, 2019, **11**, p 30163.

48. B. Kim, J. Kim, and E. Kim, B. Kim, J. Kim, and E. Kim, *Macromolecules*, 2011, **44**, p 8791.

49. F. Wang, S.W. Michael, and R.D. Rauh, F. Wang, S.W. Michael, and R.D. Rauh, *Macromolecules*, 2000, **33**, p 2083.

50. S. Bhandari, M. Deepa, A.K. Srivastava, C. Lal, and R. Kant, S. Bhandari, M. Deepa, A.K. Srivastava, C. Lal, and R. Kant, *Macromol. Rapid Commun.*, 2009, **30**, p 138.

51. R. Allen, L. Pan, G.G. Fuller, Z. Bao, and A.C.S. Appl, R. Allen, L. Pan, G.G. Fuller, Z. Bao, and A.C.S. Appl, *Mater. Interfaces*, 2014, **6**, p 9966.

52. G.M. Spinks, B. Xi, V.T. Truong, and G.G. Wallace, G.M. Spinks, B. Xi, V.T. Truong, and G.G. Wallace, *Synth. Met.*, 2005, **151**, p 85.

53. F. Hu, B. Yan, G. Sun, J.L. Xu, Y. Gu, S. Lin, S. Chen, and A.C.S. Appl, F. Hu, B. Yan, G. Sun, J.L. Xu, Y. Gu, S. Lin, S. Chen, and A.C.S. Appl, *Nano Mater.*, 2019, **2**, p 3154.

54. E.C. Cho, C.P. Li, J.H. Huang, K.C. Lee, and J.H. Huang, E.C. Cho, C.P. Li, J.H. Huang, K.C. Lee, and J.H. Huang, *ACS Appl. Mater. Interfaces*, 2015, **7**, p 11668.

55. K.Y. Shen, C.W. Hu, L.C. Chang, and K.C. Ho, K.Y. Shen, C.W. Hu, L.C. Chang, and K.C. Ho, *Sol. Energy Mater. Sol. Cells*, 2012, **98**, p 294.

56. S. Reddy, Q. Xiao, H. Liu, C. Li, C. Wang, K. Chiu, S. Ramakrishna, and L. He, S. Reddy, Q. Xiao, H. Liu, C. Li, C. Wang, K. Chiu, S. Ramakrishna, and L. He, *ACS Appl. Mater. Interfaces*, 2019, **11**, p 18254.

57. S. Xiong, R. Wang, X. Zhang, Y. Wu, Z. Xu, and Z. Chen, S. Xiong, R. Wang, X. Zhang, Y. Wu, Z. Xu, and Z. Chen, *ChemistrySelect*, 2019, **4**, p 543.

58. S. Xiong, Z. Li, M. Gong, X. Wang, J. Fu, Y. Shi, and J. Chu, S. Xiong, Z. Li, M. Gong, X. Wang, J. Fu, Y. Shi, and J. Chu, *Electrochim. Acta*, 2014, **138**, p 101.

59. D. Tasis, N. Tagmatarchis, V. Georgakilas, and M. Prato, D.
Tasis, N. Tagmatarchis, V. Georgakilas, and M. Prato,
Chemistry, 2003, **9**, p 4000.

60. F. Jia, R. Wu, C. Liu, J. Lan, Y. Lin, and X. Yang, F. Jia, R.
Wu, C. Liu, J. Lan, Y. Lin, and X. Yang, *ACS Sustain.
Chem. Eng.*, 2019, **7**, p 12591.